Materials Innovations

HEXA Publishers

Catalytic Materials | Research Article | http://doi.org/10.54738/MI.2022.21001

Biomimetic Synthesis of Highly Reusable MoO_3-based Catalysts for Fast Degradation of Azo Dyes

Irum Shaheen[1]*, Khuram Shahzad Ahmad[1]*

1 Department of Environmental Sciences, Fatima Jinnah Women University, 46000, Rawalpindi, Pakistan

OPEN ACCESS

Received: 10 August 2022

Accepted: 16 October 2022

Published: 28 October 2022

Citation: Shaheen I, Ahmad KS (**2022**) Biomimetic Synthesis of Highly Reusable MoO_3-based Catalysts for Fast Degradation of Azo Dyes. *Materials Innovations 9* (10), 255-268.

***Correspondences**: (Irum Shaheen) irumshaheen112@gmail.com (Khuram Shahzad Ahmad) chemist.phd33@yahoo.com

Published By Hexa Publishers

ISSN
Electronic: 2790-1963

Over the recent decades, unrelenting efforts are being devoted to the sustainable design and synthesis of transitional metal oxide-based photocatalysts with controlled morphology and structural complexity to enhance their catalytic properties. In this account, we have reported the bio-fuel-assisted hydrothermal synthesis of MoO_3, MoO_3:NiO, and MoO_3:PdO/Pd as catalysts to remove azo pollutants from an aqueous solution. Methyl orange was selected as the model dye to represent organic pollutants. This work presents a facile method for improving the visible-light-driven catalytic activity of MoO_3 by introducing NiO and PdO. When MoO_3:NiO and MoO_3:PdO/Pd were illuminated by solar light, emitted radiation originating from oxygen vacancies of NiO and PdO synergistically participated in catalytic reactions of MoO_3 giving 98% and 95 % degradation of methyl orange, respectively, in 15 min. To confirm the supporting role of NiO and PdO in the catalysis of MoO_3, catalytic experiments were carried out in dark ambient conditions, with only catalysts (without stimulants). Subsequently, the degradation efficiency of MoO_3:PdO, and MoO_3:NiO was increased to 73% and 84% respectively, from 62 % efficiency of MoO_3 suggesting that NiO and PdO greatly increased the efficiency of MoO_3 in dark conditions and nearly complete removal of methyl orange by photo-induced visible light degradation. Furthermore, the photocatalysts illustrated good reusability till four runs of experiments without loss in its degradation efficiency. Therefore, the overall catalytic results of the current study are highly proposing MoO_3:PdO and MoO_3:NiO as excellent photocatalysts for water remediation.

Keywords: Phytotemplate, Organic Pollutants, Photocatalysis, MoO3:PdO, MoO3:NiO, Water Remediator

INTRODUCTION

Environmental pollution, especially water pollution due to organic pollutants is becoming a life-long environmental challenge for human survival.[1−3]The major reason for water pollution is industrialization particularly industries manufacturing paper, fabrics, cosmetics, leather accessories, etc. Azo dyes are widely used in these industries.[4−5]Consequently, the removal of azo dye pollutants from water is extremely important to protect human health and also to protect the aquatic environment.[5−8] In the recent past photocatalysis of organic pollutants such as azo dyes is being reported as the most successful method to remove and degrade organic dyes from water bodies.[5−12] The photodegradation

with help of solar light and semiconductor materials (such as metal oxides) is greatly investigated in dealing with environmental issues related to organic pollutants. [3–7,10–12]

Among the different semiconductors materials (ZnO, TiO_2, Co_3O_4, etc), molybdenum trioxide (MoO_3) is the most competitive photocatalyst. It is n-type material having a floating direct band gap (2.3 to 3.6 eV), and is the most fascinating transition metal oxide due to its unique double-layered planar structure, higher chemical stability, and nontoxicity.[13] MoO_3 has high photogenerated charge transfer efficiency due to its narrow bandgap and solar light absorption. Thus, MoO_3 has a high potential for photocatalysis and solar cell applications. Recently, MoO_3 has been extensively investigated as a photocatalyst for the degradation of dyes.[13–17] Hussain and Khalid, 2020 synthesized MoO_3 via a surfactant-assisted synthesis route for photo-degradation of different organic dyes (methylene blue, rhodamine B, and alizarin). The results of their study revealed 98%, 90%, and 74% degradation of methylene blue, rhodamine B, and alizarin respectively within 120 min by MoO_3.[13] In another study, Al-Alotaibi et al., investigated the catalytic efficiency of MoO_3 synthesized by sol-gel and hydrothermal method for degradation of methylene blue. They demonstrated the complete degradation of methylene blue within 180 min.[14] Moreover, MoO_3 film was prepared by Zhang et al., for the degradation of methylene blue and they reported its degradation efficiency of with150 min.[15] Although effective degradation of dyes by MoO_3-based catalysts is well reported in literate. However, the time taken to remove organic dyes is equally important. In order to enhance the efficiency of MoO_3 to degrade organic dyes, MoO_3 has been synthesized in combination with other metal oxides and nano materials. Such as Kamalam et al., prepared nanocomposites of α-MoO_3 /Graphene Oxide (GO) and studied it for degradation of Victoria blue dye in visible light irradiation. They showed 89% efficiency of GO/MoO_3 for the removal of organic dyes in 150 min.[16] In another study, Huang et al., synthesized molybdenum oxide (MoO_3) nanorods decorated with molybdenum phosphide quantum dots and reported its 100% degradation efficiency within 40 min for Rhodamine B dye and 97% efficiency for norfloxacin dye.[17]

Therefore, the present study is also an attempt to overcome the challenge of faster degradation of organic pollutants. For this purpose, in the current study, NiO and PdO were synthesized in MoO_3 semiconducting material to degrade methyl orange (hereafter called "MO") in water. NiO is a p-type semiconducting material having a wide band gap which is making it apt as a photocatalyst application. Due to the higher hole mobility of NiO, it can degrade organic dyes in a shorter time under solar irradiation.[18] Pd and PdO exhibit higher catalytic activity at lower temperatures. It is reported that incorporation of PdO with other transitional metal oxides (TMOs) results in superior photocatalytic behavior of TMOs. [19] Such a study is reported by Zhou et al., where they synthesized PdO–TiO_2 nanocatalyst which exhibited tremendously high photocatalytic potential for degradation of methylene and rhodamine B.[20] Therefore, in the current study MoO_3, MoO_3:NiO and MoO_3:PdO were synthesized using phytochemicals of *A.pindrow* leaves as template and fuel. Phytochemicals, not only as reducing but also as stabilizing agents, have been critically investigated.[21–23] In our previous study, we have successfully synthesized Co_3O_4 based photocatalyst by *A.pindrow* plant leaves for degradation of azo dye.[24] Therefore, the current research was the first attempt to synthesize MoO_3, MoO_3:NiO, and MoO_3:PdO/Pd using phytochemicals of *A.pindrow*. In the current experimentation, the hydrothermal method was used employing Phyto reducing and stabilizing agents. In the current experiment, hydrothermal reactions were initially carried out at 70 ^{o}C and final MoO_3 was obtained by calcination in air at ~ 400 ^{o}C. Moreover, the cost-effective and efficient hydrothermal synthesis route was adopted in the current experiment employing green reducing cum stabilizing agents to replace costly and hazardous chemical reagents and solvents. These organic compounds of *A.pindrow*, as stabilizing agents, incorporate into synthesized material increasing O and C atoms in the mediated materials to enhance their photocatalytic activity. In the present work, MO has been degraded using MoO_3, MoO_3:NiO and MoO_3:PdO/Pd with maximum degradation efficiency in 15 min. To the best of our knowledge, we have demonstrated the maximum degradation of MO using MoO_3-based catalysts in a shorter time of 15 min due to the addition of NiO and PdO as well as by increased O and C atoms of bioactive compounds.

MATERIALS AND METHODS

Chemicals and Materials

The precursors used in the current study were Molybdenum acetate ($Mo_2(O_2CCH_3)_4$), nickel(II) acetate tetrahydrate ($Ni(CH_3CO_2)_2{\cdot}4\ H_2O$), Palladium acetate (($Pd(CH_3COO)_2$). For catalytic experiments, methyl orange (MO) ($C_{14}H_{14}N_3NaO_3S$) was used. All chemicals were purchased from Merck chemicals Ltd. The solvent used in the present study was deionized water. Leaves extract of *A.pindrow* was used as synthesizing agent.

Synthesis of Materials

The detailed methodology has been reported in our recent study[24] and was adopted to synthesize MoO_3, MoO_3:NiO and MoO_3:PdO materials with little modifications. In brief, 1 g of *A.pindrow* powdered leaves were

treated in 50 mL of deionized water at 60 ^{o}C and 600 rpm for 30 min and then filtered. 10 mL of filtrate was added as fuel into 100 mL of 20 mM $Mo_2(O_2CCH_3)_4$ aqueous solution on magnetic stirring. The reaction mixture was kept at 70 ^{o}C for 2 h at 550 rpm and then retained at room temperature in dark conditions for 24 h. Afterward, the solution was evaporated at 95 ^{o}C to get dry powder which was annealed at 460 ^{o}C for 4.5 hours to obtain MoO_3. The calcinated MoO_3 was suspended in deionized water in two different beakers. In one beaker of prepared MoO_3 suspension, the aqueous solution of $Ni(CH_3CO_2)_2{\cdot}4H_2O$ was added, and in other beakers, $Pd(CH_3COO)_2$ aqueous solution was added. The ratio of MoO_3:NiO and MoO_3:PdO/Pd were carefully controlled in 8:2. Therefore, 20 % $Ni(CH_3CO_2)_2{\cdot}4$ H_2O and 20 % $Pd(CH_3COO)_2$ were added in the suspension of MoO_3. In each reaction, 5 mL of *A.pindrow* extracted phyto-reagents was added and was kept at constant stirring for 2 h at 80 ^{o}C. Then, reactions were evaporated completely at 96 ^{o}C before calcinating at 450 ^{o}C for 3.5 h to obtain MoO_3:NiO and MoO_3:PdO.

Catalytic degradation of methyl orange (MO)

In the present catalytic experiment, MO was taken as an organic pollutant. Solar radiations were used to provide visible light. The measured quantity of 2 mg of each prepared material was added to 15 mL of MO solution (1 mg/mL), on magnetic stirring for 60 min to achieve reaction equilibrium. After then the solution was subjected to visible light radiation for 15 min. During the process, a small amount of solution was taken regularly to monitor MO concentration by UV Vis spectrophotometer at 464 nm. To study the effects of visible light on the degradation of MO, a dark experiment was also run, for that three centrifuge tubes were taken and covered entirely by Aluminium foil to avoid interference of any type of stimulant. In one tube 2 mg MoO_3 was added and in the other two tubes, the same amount of MoO_3:NiO and MoO_3:PdO/Pd were added. In each tube, 15 mL of MO solution was added and then left at room conditions for 15 min. The degradation of MO in dark mild conditions was also observed at equal time intervals as for light experiments. Moreover, an aliquot from the stock solution of MO was taken and subjected to the same light and dark experimentation as a blank sample to appraise the meticulous efficiency of the catalysts. After completion of each experiment (i.e. after every 15 min) catalysts were recovered, dried, and tested for another run of the experiment to investigate the reusability potential of the bio-synthesized materials.

Characterization

Each synthesized material was keenly investigated for its structural, compositional, and morphological properties by numerous analytical instruments and techniques as described in our recently published work.[24]The catalytic experiment was monitored by ultraviolet-visible spectrophotometry 1602-BS, Spain (UV-Vis). The gas chromatography coupled with mass spectroscopy (instrument model: GC-MS-QP5050) (GCMS) and FTIR-8400S was used to study the organic constituents of synthesized materials. PANalytical X'Pert Pro-XRD5 (X-ray powder Diffractometer (XRD), Quanta FEG-250 SEM (an environmental Scanning Electron Microscopy (FE-SEM)) coupled with energy-dispersive X-ray microanalysis (EDX) and Renishaw's Raman systems (Raman spectroscopy) were employed to study phase, morphology, and composition of mediated nanomaterials.

RESULTS AND DISCUSSION

Phyto-synthesized materials

The annealed powders of MoO_3, MoO_3:PdO, and MoO_3:NiO were explored by FTIR and subsequent spectra are annotated in Figure 1(a-c). In all synthesized materials, vibrational peaks corresponding to O-H stretch (phenol, alcohol) were found at 3448.84 cm^{-1}, 3457.47 $cm^{-1,}$and 3490.06 $cm^{-1}$for MoO_3, MoO_3:PdO, and MoO_3:NiO respectively. This revealed the incorporation of phenolic compounds in the synthesized materials. However, MoO_3 NPs (Figure 1(a)) revealed the presence of aromatics (C-C stretch in ring and C-H "oop) at 1648.14 $cm^{-1}$and 1437.8 cm^{-1}, 855.7 cm^{-1}, and 791.8 cm^{-1}respectively. In Figure 2(b) vibrational frequencies of MoO_3:PdO at 1648.14 cm-^{1}, 1028.9 cm^{-1}, 786.71 cm^{-1}, 560.89, and 439.9 cm^{-1}corresponding to C-C stretch of aromatics, N-H stretching relating to aliphatic amines, C-H "oop" of aromatics and M-O bond of metal oxides (M = Mo, Ni, Pd) respectively.[25–26]M-O bonds were also demonstrated in MoO_3:NiO (Figure 1c) at 567.8$cm^{-1,}$whereas in MoO_3:NiO aromatics groups were also observed at 1622.13 cm^{-1}, 989.5 cm^{-1}, and 871.44 cm^{-1}(C-H "oop") while the minor peak at 1377.52 $cm^{-1}$was indicating the presences of nitro compounds as it depicts the presences of N-O groups.

From Figure 1(a-c) it is shown that aromatic functional groups of phenol compounds are present in the synthesized materials. However, to confirm these belong to bio-organic compounds of the plant leaves, MoO_3, MoO_3:PdO, and MoO_3:NiO were studied by GC-MS and the resulting spectra have been annotated in Figure 1(d-f). According to NIST library of GC-MS-QP5050, the peaks of figure 1d are illustrating the cyclobutanol (C_4H_8O) in MoO_3 nanoparticles. While Benzeneethanamine ($C_8H_{11}N$), Benzenemethanol ($C_9H_{13}NO$) Benzeneethanamine ($C_8H_{11}N$), and cyclobutanol were predicted in MoO_3:PdO (Figure 1(e)) at 4.7 min, 4.9 min, 5.4 min and 20.4 min retention times respectively. MoO_3:NiO in Figure 1(f) depicts the incorporated compounds at

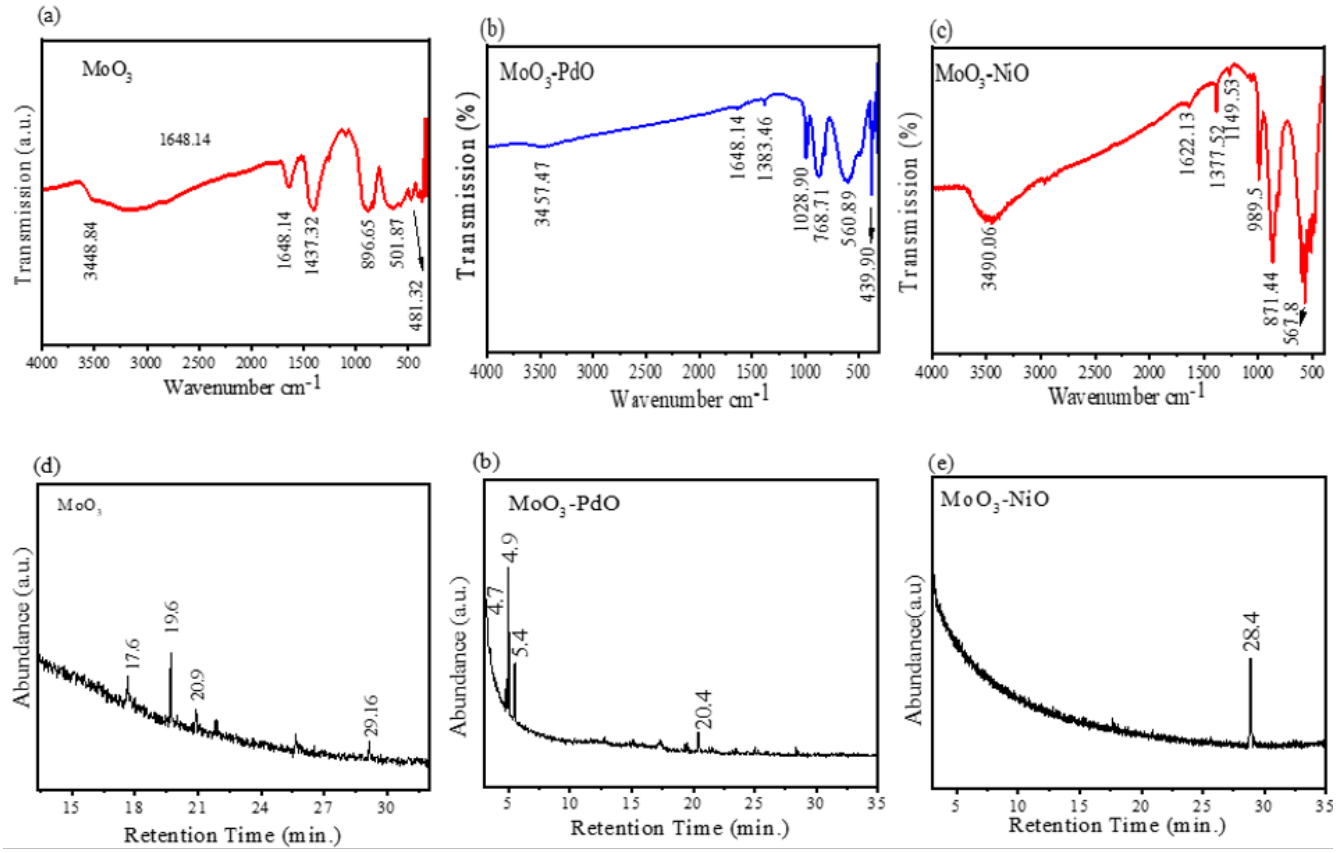

Figure 1. MoO, (b) MoO:PdO and (c) MoO(d) MoO, (e) MoO:PdO and (f) MoO:NiO.

28.4 min retention time, corresponding to cyclobutanol. Therefore, GCMS has validated the FTIR peaks interpretation that the aromatic organic phenolic compounds are present in the synthesized materials. The proposed compounds by GC-MS are allied with *A.pindrow* phytochemicals which has been reported in our recent study.[24] The carbon/oxygen functional groups will in turn enhance the visible-light-induced degradation of the catalysts due to their hydrophilic nature and the higher negative charge densities. These features of carbon/oxygen functional groups can facilitate the degradation of azo dye by augmenting the separation between electrons and holes during photocatalysis.[36–37]

Further, MoO_3, MoO_3:PdO, and MoO_3:NiO were studied by Raman spectroscopy (Figure 2). All the images in Figure 2 are suggesting MoO_3 as key constituents of the phytosynthesized materials, as Raman scattering vibration of Figure 2 are well matched with reported Raman spectra of MoO_3 by Krishna et al.,[27] Joya et al.,[28]Liu et al.[29] The presence of NiO and PdO in figure 2b and Figure 2c is determined by comparing the spectral vibrations with reported Raman scattering vibrations of NiO and PdO by Ren et al.,[35] and Korifi, et al.,[39]respectively. Nevertheless, the increased concentration of organic compounds in the MoO_3:PdO can be speculated in the Raman scatterings of MoO_3:PdO in Figure 2(c) as demonstrated by the GC-MS spectrum in Figure 1e. GC-MS analysis of MoO_3:PdO illustrated more than one organic compound. Moreover, Figure 1e revealed the higher peak intensities of organic species as compounds to figure 1d and Figure 1f of MoO_3 and MoO_3:NiO respectively. Therefore, MoO_3:PdO showed a noticeably changed spectrum of Raman over 300–3000 cm^{-1} due to different organic compounds of *A.pindrow* template. However, determined phases from Raman scatterings vibrational patterns of synthesized materials were further endorsed by X-ray diffraction patterns as given in Figure 3.

X-rays diffraction patterns are indicating the phyto-synthesis of MoO_3, MoO_3:PdO, and MoO_3:NiO materials by scrutinizing their phase purity dimensions and by estimating their crystallite sizes. The diagnosed patterns in XRD spectra in Figure 3(a) are depicting the MoO_3 phase of bio-mediated nanoparticles according to JCPDS:00-005-0508. Standards patterns further revealed that MoO_3 particles were crystallized with Orthorhombic, molybdite, syn (with lattice parameters a= 3.962, b= 13.858,

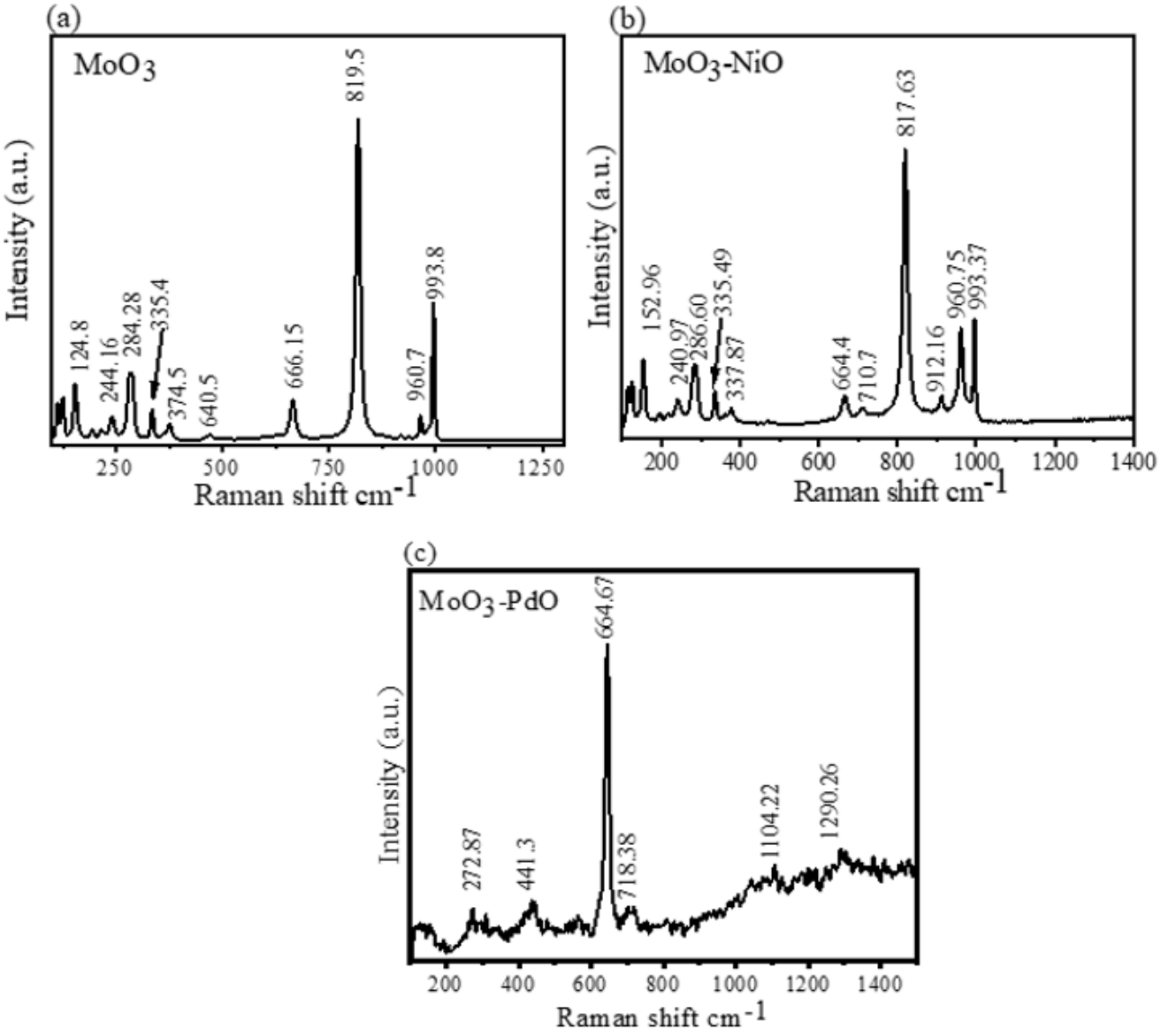

Figure 2. Raman spectra of organic compounds derived nanomaterials: (a) MoO_3, (b) MoO_3:NiO and (c) MoO_3:PdO.

and c = 3.697). Figure 3b shows diffraction patterns of MoO_3:PdO nanomaterial. MoO_3produce the peaks in figure 3b (*) at 12.6329^o (020), 23.2225^o(110), 25.5116^o (040), 27.225o (021), 33.138^o (101), 33.569^o(111), 35.4385^o (041), 38.8161^o(060), 45.0736^o(200), 46.2775^o(210), 49.2687^o (002), 52.3683^o(211), 55.1159^o(112), 56.3964^o (042), 57.4644^o(171), 58.5905^o(081), 64.7541^o(062), and 69.5093^o(202) with respective hkl planes Moreover the X-rays diffractogram in Figure 3(b) also revealed the presence of tetragonal PdO (♦) at 29.317 (100), 33.55 (002), 33.84 (101), 41.93 (110), 45.139 (102), 60.22 (103), 60.75 (200), and 71.46 (211) (ICSD:00-041-1107) with P42/mmc space group and unit cell parameters of a = 3.0456 Å, b = 3.0456 Å and c = 5.3387 Å. Figure 3(c) shows the XRD patterns of bio-organic compounds derived MoO_3:NiO. The diffraction patterns in Figure 3(c) show well-defined prominent peaks of molybdenum oxide-MoO_3 (ICSD 00-005-0508) as well as NiO oxides (ICSD:00-047-1049). The X-ray diffractogram has shown that MoO_3 peaks (*) at 2theta (^{o}) = 12.775, 23.41, 25.67, 27.38, 33.81, 35.48, 38.95, 46.39, 49.36, 52.75, 54.19, 56.44, 57.75, and 58.79 corresponding to hkl planes of (020), (110), (040), (021), (111), (041), (060), (210), (002), (211), (112), (042), (171), (081), (062), and (190) respectively. While the presence of NiO (●) in Fig-

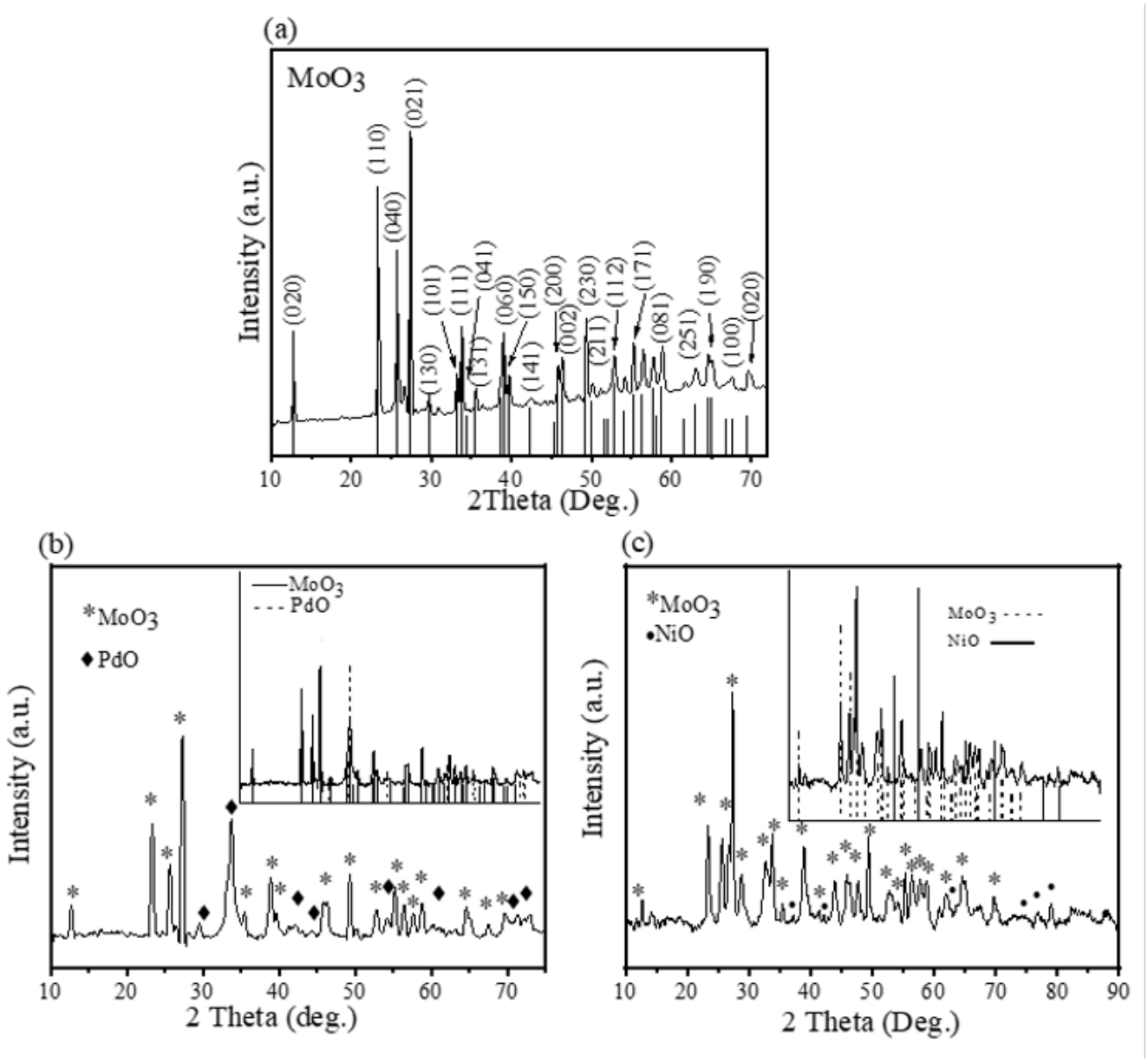

Figure 3. X-rays diffraction patterns of A.pindrow assisted (a) MoO_3, (b) MoO_3:PdO, and (c) MoO_3:NiO.

ure 3c was indicated at 2 37.3^o(111 hkl), 43.2^o(200 hkl), 62.8^o(220 hkl). The crystallite sizes of all synthesized samples were calculated via Scherrer's equation as described in our earlier study.[25]The calculated sizes of MoO_3 was 40-43 nm, MoO_3:PdO had 31-33 nm while MoO_3:NiO had 19-21 nm crystallite size. XRD certified the phytosynthesis of MoO_3, MoO_3:PdO, and MoO_3:NiO material while the elemental composition of synthesized material was investigated by Energy Dispersive Spectroscopy (EDX) as given in Figure 4.

In Figure 4(a), EDX revealed the presence of O and Mo with atomic % of 74.11 and 21.39 respectively along with 4.3% carbon. Figure 4(b-c) also presents the presence of C in both MoO_3:PdO and MoO_3:NiO. The presence of C is due to the phytochemicals of *A.pindrow* extract proposing the phyto stabilization of MoO_3, MoO_3:PdO, and MoO_3:NiO. These results of EDX are well in agreement with Figure 1 where organic functional groups were described.

Figure 5 shows the uniform arrangements and regular structures of particles at different magnifications by FE-SEM. The uniform pattern and regular structures of MoO_3, MoO_3:PdO, and MoO_3:NiO are particularly observable at lower magnifications in Figure 5a, Figure 5(d), and Figure 5(g) respec-

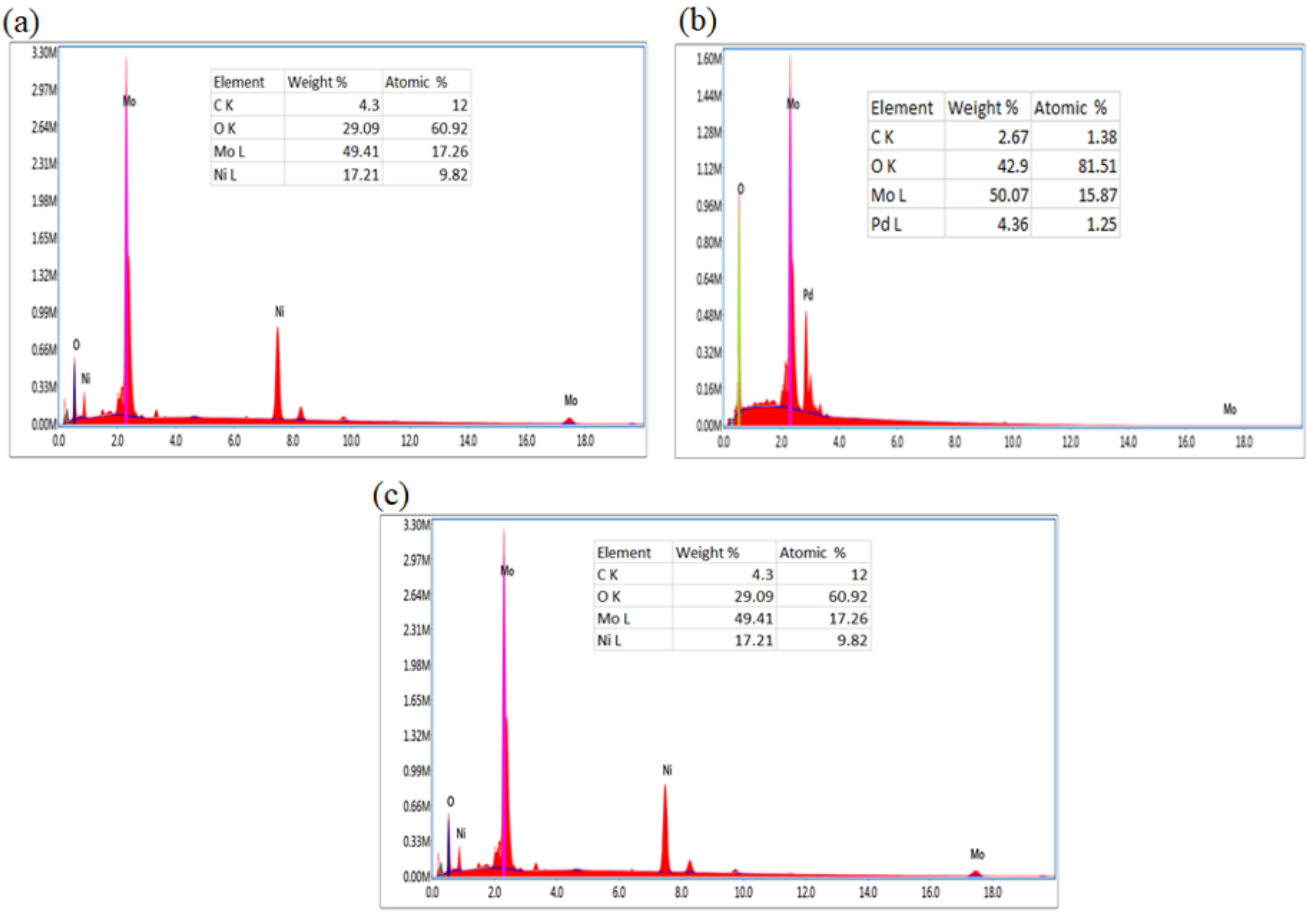

Figure 4. Elemental composition of A. pindrow assisted (a) MoO_3, (b) MoO_3:PdO, and (c) MoO_3:NiO Via Energy Dispersive Spectroscopy.

tively. From Figure 5a-c, rod-like structures of MoO_3 particles can be speculated at 5 μm to 1 μm scales. Figures 5(d-e) are presenting 5 μm, 2 μm, and 1 μm structures of MoO_3:PdO with non-homogeneous shapes but Figure 5d-e is correspondingly showing some porosity in these particle's structures due to embed PdO. Upon the introduction of NiO and by re-thermal annealing (Figure 5(g-i)), MoO_3 morphology has greatly changed into sheet-like structures with spherical-shaped NiO. Agglomeration is generally occurred in doped materials especially at the nanoscale, however, from Figure 5 it can found that synthesized MoO_3:PdO (Figure 5f)and MoO_3:NiO (Figure 5(i)) materials are showing less agglomeration at 1μm and 500 nm, respectively. This is suggesting the role of stabilizing agents of the plant leaves biochemical as reported extensively in the literature.[22–26]

Degradation study of MO by synthesized materials

The catalytic activity of the biosynthesized MoO_3, MoO_3:NiO, and MoO_3:PdO catalysts was scrutinized by MO degradation in the water under solar light radiations at the room temperature. The concentrations of MO were taken at 1 mg/mL and catalysts loading was controlled at 2 mg/15 mL. The catalytic behavior of MoO_3:NiO and MoO_3:PdO was investigated in comparison with MoO_3. The λ_{max} of MO was reported at 464 nm,[30,31,37,38]thus, absorbance intensity at 464 nm was observed critically to determine the amount of MO degraded by the fabricated catalysts using the equation reported previously.[24]

As shown in Figure 6, absorption intensity decreases with the increment of time. The UV/Vis measurements of synthesized catalysts were taken at a range of time intervals from 0 to 20 min, and subsequently, absorption curves were delineated at 2, 5, 10, and 15 min. Reduction in absorption is due to the breakage of azo bonds by synthesized nanomaterials in the presence of light (Figure 6(a-c)) and dark conditions (Figure 6(d-f). The absorption spectra are depicting that MO peaks are significantly reduced with solar light stimulants than without solar light stim-

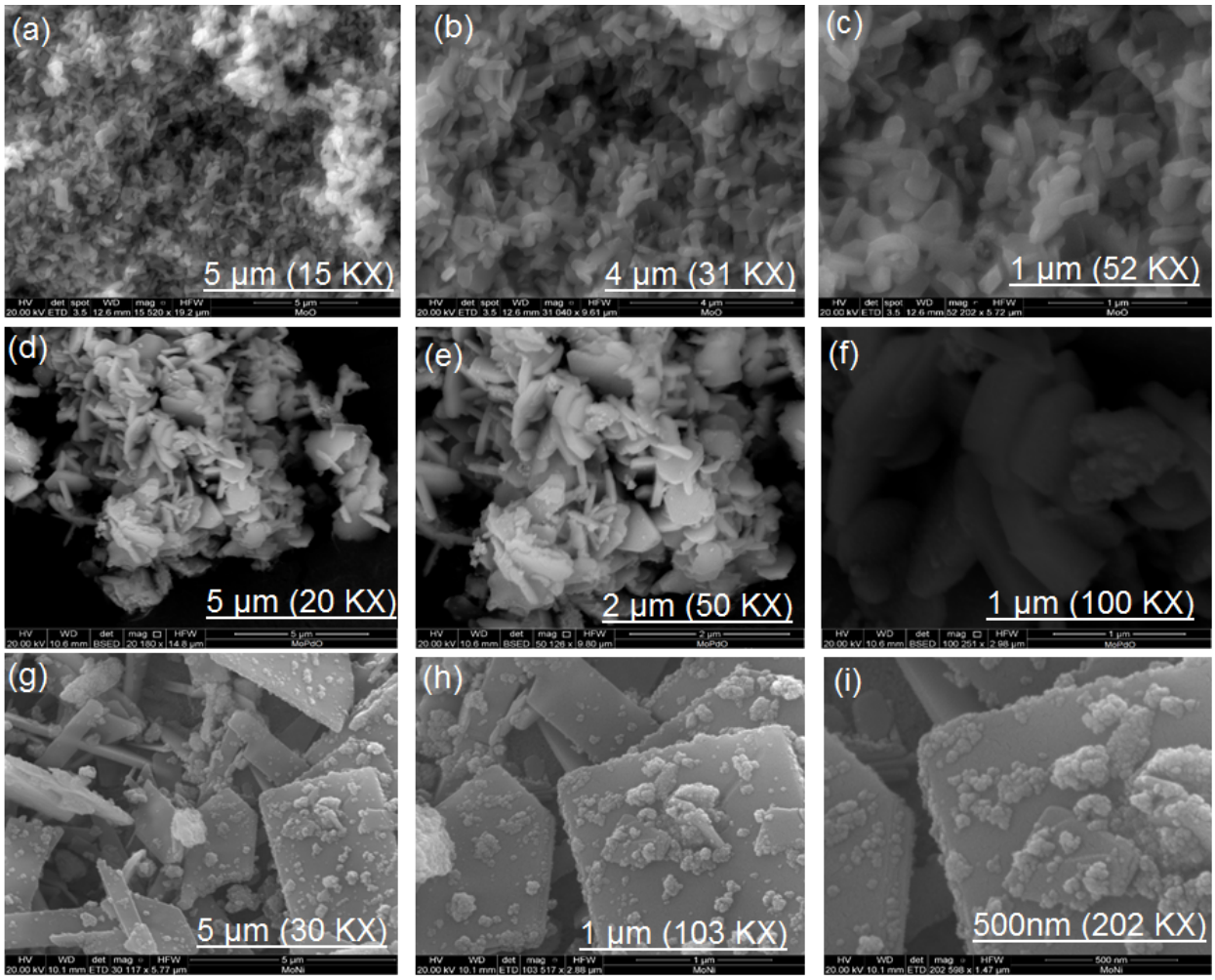

Figure 5. FE-SEM images A.pindrow synthesized materials at different magnifications (a) MoO_3 at 15KX , (b) MoO_3 at 31KX , (c) MoO_3 at 52KX, (d) MoO_3:PdO at 20KX, (e) MoO_3:PdO at 50KX, (f) MoO_3:PdO at 100KX, (g) MoO_3:NiO at 30 KX, (h) MoO_3:NiO at 103KX, and (i) FESEM images MoO_3:NiO at 202 KX.

ulants (under dark conditions). It can be seen in Figure 6c that the absorbance peak completely disappeared till 15 min by MoO_3:NiO where the degradation was simulated by Visible light while MoO_3:PdO also revealed a great reduction in absorption as compared to MoO_3. It is worth describing that in Figure 6d the absorption of the MO (without catalysts) is considerably higher in both light and dark as compared to Figure 6. Thus, the reduction in absorption intensities in Figure 6 is associated with the catalysis potential of the synthesized materials. However, higher reduction in Figure 6 (b, c) and in Figure 6 (e and f) is indicating that introduction of Ni and Pd in MoO_3 has shifted the electronic structure of MoO_3 by the formation of NiO and PdO in MoO_3 which have enhanced the efficiency of MoO_3 to degrade MO, as also revealed in Figure 7 and Table 1. According to table 1, the self-photodegradation of MO was only 5 % till 15 min and almost no degradation was observed under ambient conditions, this has further supported the role of mediated materials in degrading MO.

Table 1 and Figure 7(b) show 80% and 85% degradation of MoO_3 with the help of solar light in 10 and 15 min whereas without visible light (in dark room conditions) only 48 % and 62 % MO were degraded in the same time. However, by doping of PdO in MoO_3 photodegradation of MO was increased to 66 % and 95 % in 10 and 15 min respectively as presented in Figure 7(c). Under dark conditions, 73 % degradation was observed after 15 min by MoO_3-PdO. The highest degradation (98 %) was observed when NiO was incorporated in MoO_3 with solar light stimulation. Even after 2 min, 72.23 % degradation of MO was found assisted by visible light while after 5 min 86 % removal of MO was observed by MoO_3:NiO which is higher than 85 % degradation of MO by only MoO_3

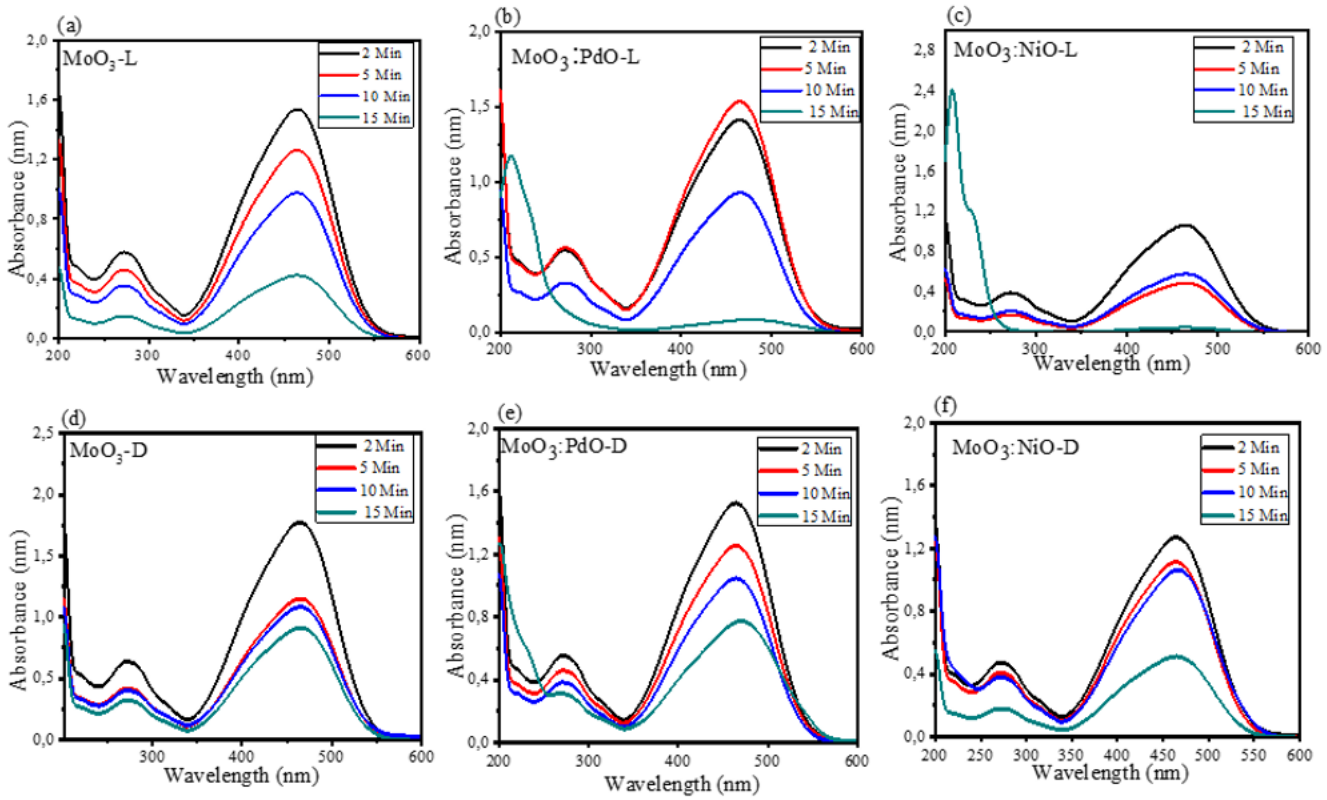

Figure 6. UV/Vis spectra of MO photo-degradation by (a) MoO_3, (b) MoO_3,:PdO, (c) MoO_3:NiO, and MO degradation without stimulant under dark conditions of (d) MoO_3, (e) MoO_3:PdO, and (f) MoO_3:NiO.

Table 1. Degradation of azo dye calculated for each synthesized catalyst and for blank sample.

	MoO_3 (%)		MoO_3-PdO (%)		MoO_3-NiO (%)		Blank (%)	
Time (Min)	Visible Light	Ambient condition	Visible Light	Ambient condition	Visible Light	Ambient condition	Visible Light	Ambient condition
2	44.5	40.7	48.19	47.2	72.23	54.57	0	0
5	64.5	25.89	44.49	63.9	86.3	63	2	0
10	80.4	48.12	65.95	67.7	94.5	68.5	5	2
15	85.2	62.4	95.3	73.1	98	84.85	5	0.5

sample after 15 min. Not only by solar irradiation, MoO_3:NiO revealed the highest degradation of ~ 85 % in dark conditions. Thus, MoO_3:NiO has huge potential as a catalyst (particularity as a photocatalyst) for the degradation of MO due to the combination of p-type NiO and n-type MoO_3 as well as due to nanoscopic features of MoO_3:NiO as described in Figure 5(g-i). The Fermi equilibrium (at the p-n junction) is inhibited the recombination of photo-generated charge carriers (e^-/h^+) to prolong their separation, consequently increasing the photocatalysis.[35,37–38]

The experiments of degradation of MO under solar irradiation showed superior catalytic efficiency of MoO_3:PdO and MoO_3:NiO (with 2 mg catalyst in 15 mL of dye solution of 100g/L) than the photocatalytic activity of molybdenum doped TiO_2 nanostructure (dye 0.02M and 1.36% catalysts)[33] MoO_3 (having 250 mg per 250 mL catalyst and dye amount),[16]ZnO/MoO_3 nanotubes (0.3 g/L dye and 1 g catalyst),[15] and Mo-doped TiO_2 (20 mg/L MO solution and 0.5 g catalyst).[17]The enhanced photo-catalytic activity can be due to carbon phytochemicals which retard the recombination of holes and electrons in the presence of light.[38–39] Thus, it can be concluded that the carbonaceous functional groups of Phyto template may have a significant role in improving the catalytic activity in the presence of light radiation.

From Figure 8, it can be notable illustrated that $\ln(C_0/C)$ varies linearly with the reaction time accordingly, the kinetics of MO degradation is consistent with the pseudo first-order reaction model. The regression values (R^2) for MoO_3, MoO_3:PdO, MoO_3:NiO in light irradiation were

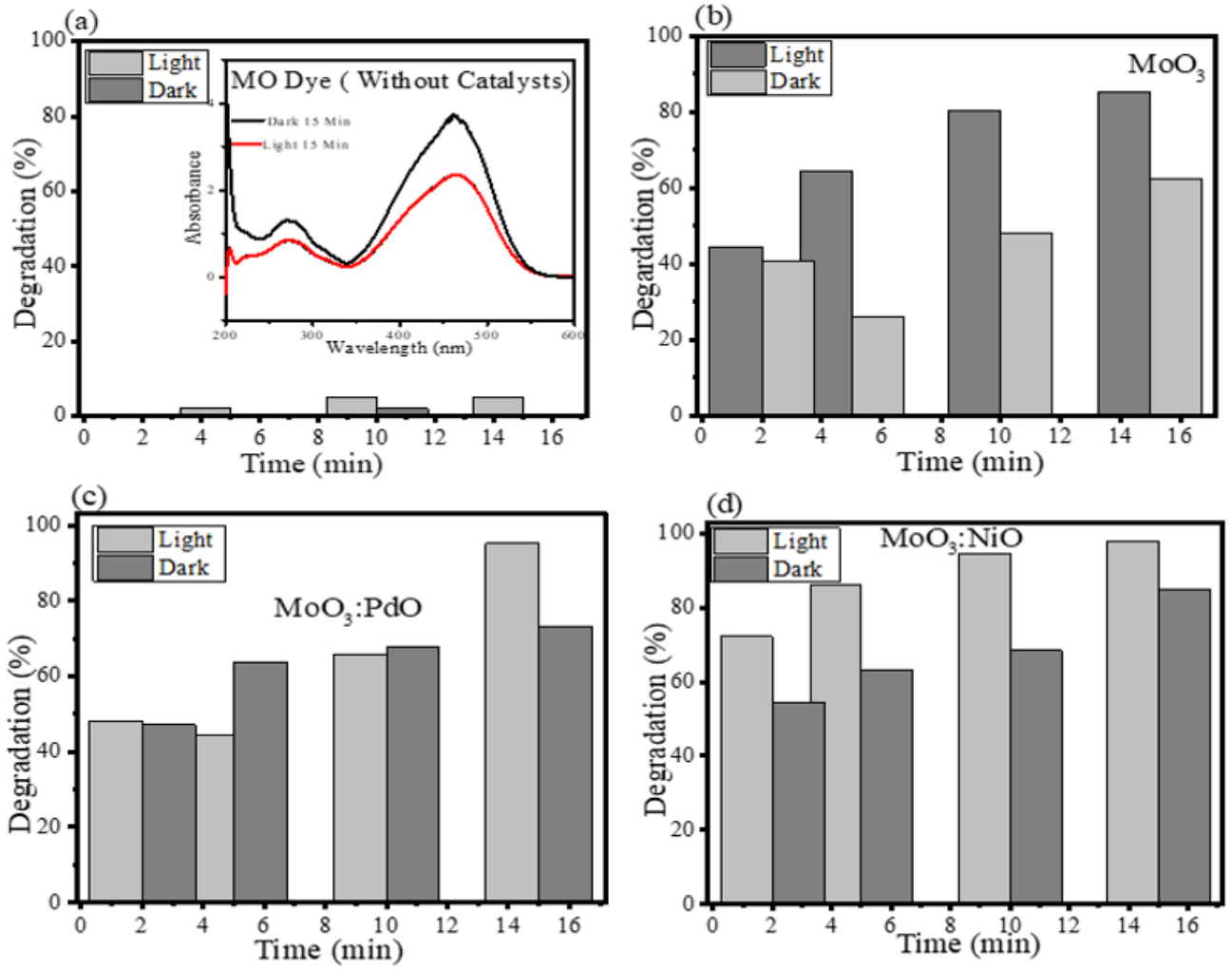

Figure 7. (a) Percentage degradation of MO without catalysts at different time intervals (insert: absorption spectra of MO without catalysts in light and in dark), the calculated degradation percentages of MO by synthesized nanomaterials: (b) MoO_3, (c) MoO_3:PdO, (d) MoO_3:NiO.

0.88, 0.89 and 0.8 respectively while R^2= 0.65, 0.96, and 0.74 were found for MoO_3, MoO_3:PdO, MoO_3:NiO respectively for the dark catalytic reaction. The results of regression analysis of MoO_3:PdO (Figure 8(e-f)) were depicted. MoO_3:PdO was stable catalysis with and without solar light stimulating conditions while all catalysts showed primary stability with the application of solar light.

The stability and reusability of catalysts are a key important factor for the evaluation of their practical application.[31,39]Thus, the synthesized catalysts were tested for different cycles of photocatalytic performance. The catalytic performance of MoO_3, MoO_3:PdO, and MoO_3:NiO till four runs is shown in Figure 9(a-c) respectively in the presence of solar irradiation. The photocatalytic efficiency of the fabricated catalysts was remarkably maintained till the fourth run, as no change in the absorbance values was recorded in Figure 8. Thus, reusability experiments were demonstrating that tested catalysts retain excellent stability in terms of catalytic performance.

Degradation mechanism

In the present experimentation, the possible process for degradation of MO over semiconducting MoO_3 in the presence of visible light radiation is a photocatalytic process, in which light-induced electron and hole existing over MoO_3 with $O_2$and OH– to form oxidants • O_2 and • OH^-, respectively, which then react with organic compounds and degrade them. In the MoO_3:PdO and MoO_3:NiO increased oxygen valances are accountable for the degradation process by the mechanism of chemical wet oxidation

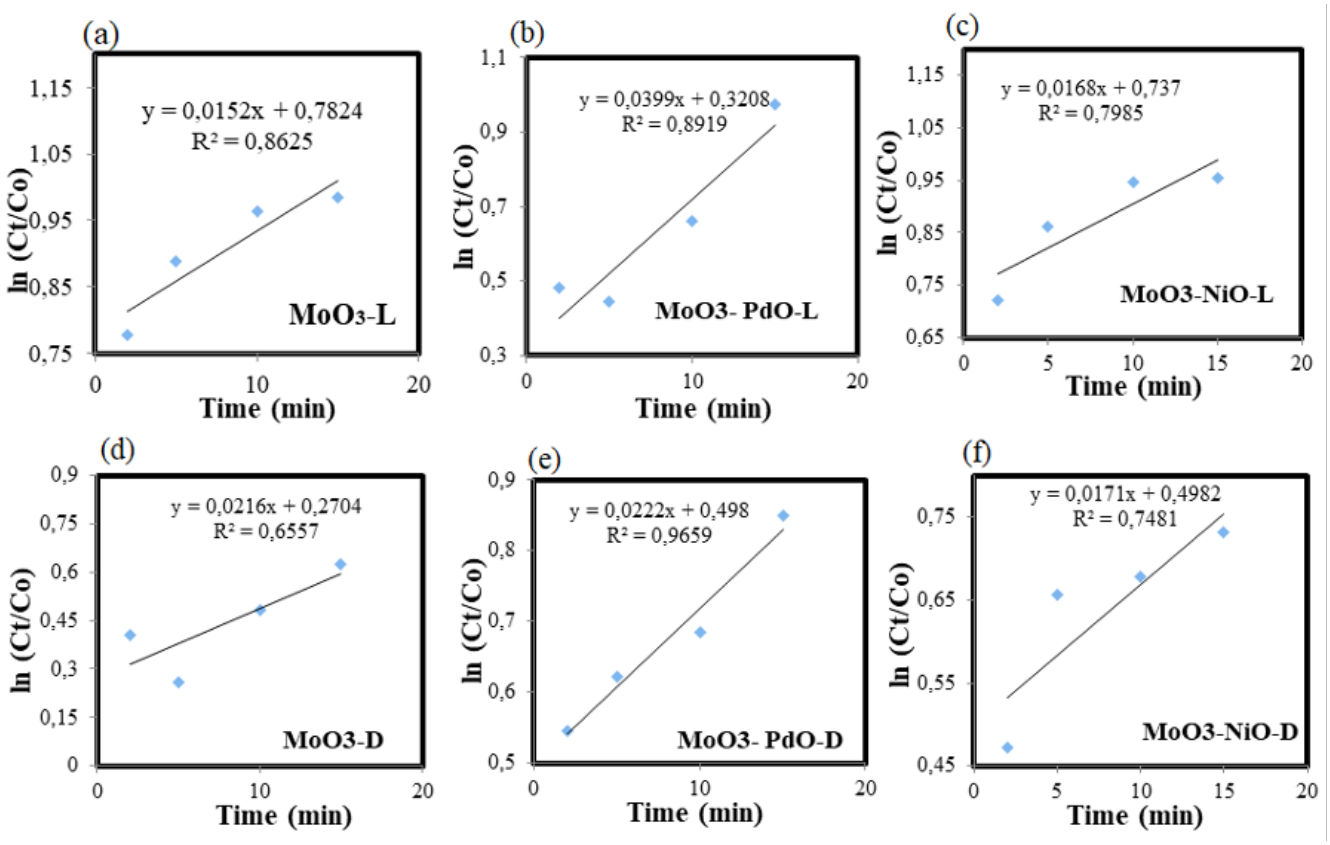

Figure 8. Degradation Reaction kinetics of investigated catalysts under solar light: (a) MoO_3 (b) MoO_3:PdO, (c) MoO_3:NiO and Degradation Reaction kinetics of investigated catalysts under dark conditions (d) MoO_3, (e) MoO_3:PdO (f) MoO_3:NiO.

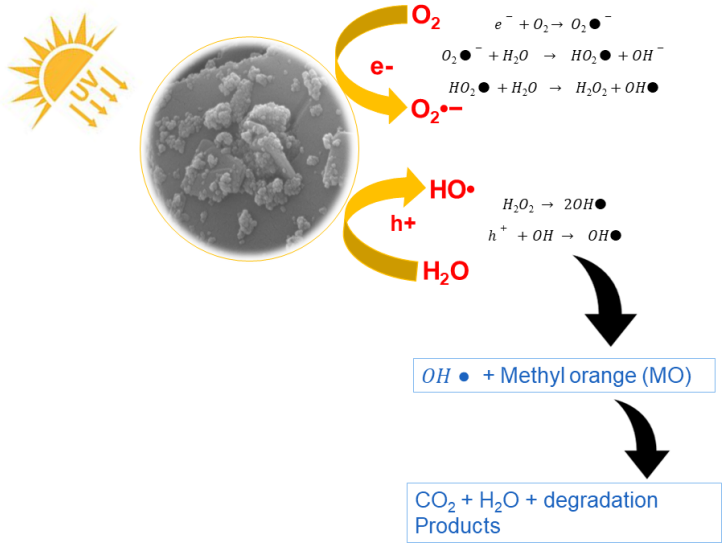

Scheme 1. Photocatalysis mechanism of MoO_3:NiO assisted dye degradation.

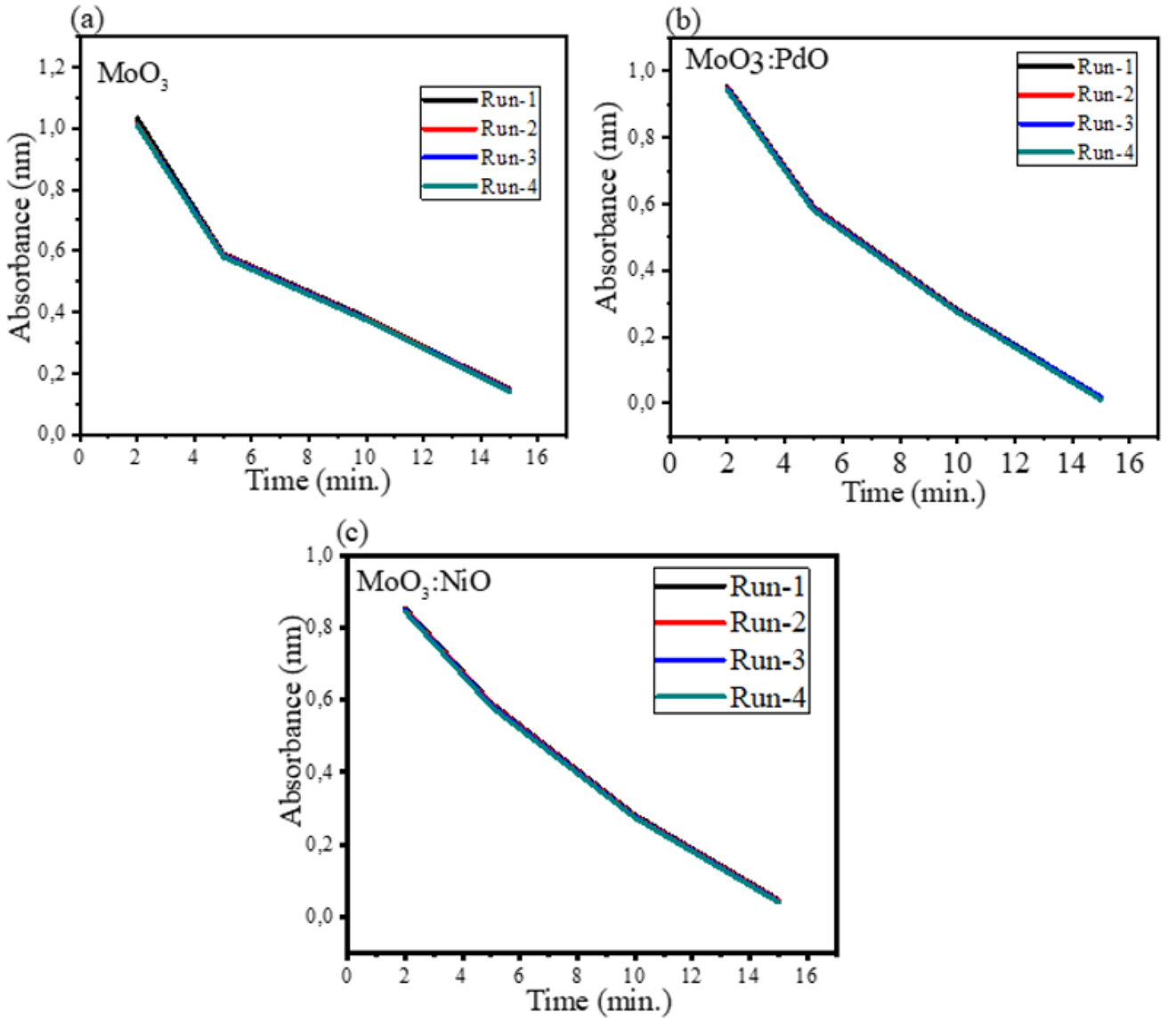

Figure 9. Different cycles of photodegradation experiments of MO by (a) MoO_3, (b) MoO_3:PdO and (c) MoO_3:NiO.

(CWO). This mechanism is described previously by Huang et al.,[15] Li et al.,[36]and Srikhaow and Smith.[37]

In the present study, the process of photocatalysis was accelerated by the carbon of phytochemicals. As Reddy et al.,[35]described that carbon is an efficient electron acceptor while semiconducting materials like MoO_3, are strong electron donors. The incorporated carbon-based phytochemicals (revealed by GC-MS) eased the flow of the charge carrier in opposite direction in the presence of photo-irradiation for efficient utilization of light for the degradation of azo dyes. Thus, depending on holes as well as electrons of MOs along with inserted carbon comprising materials, the mechanism of MO degradation can be described in reaction scheme 1.[5]

As shown in above scheme 1, electrons were produced by solar light and by the oxidation process. Freely transferred from the conduction bands to the surface of catalysts which is composed of mixed metal oxides and carbon and oxygen-containing atoms which then bind with conjugated MO molecules. At the same time, holes produced by photons as well as the CWO process persisted in the valence band and then get trapped by hydroxyl groups present on the catalyst surface to contribute OH● radicals. After this, dissolved oxygen reacted to electrons of carbon (e^-) and gave O_2● $^-$(superoxide radical anion). O_2● $^-$ after protonation produced hydroperoxy radicals (HO_2●) that were robust OAs in MO degrading, accordingly, improving catalytic action of the synthesized material. Conse-

quently, the generated holes, hydroxyl free radicals as well as superoxides of • OH and • O_2 are responsible for the efficient degradation of MO.

CONCLUSIONS

In this work, the visible-light supported the catalytic activity of MoO_3, MoO_3:PdO and MoO_3:NiO, which was investigated to degrade MO. MoO_3 was synthesized by low-cost and green template of A. pindrow and then NiO and PdO were separately synthesized in MoO_3 in the presence of biofuel. The introduction of PdO and NiO greatly improved the catalytic activity of MoO_3. The photocatalytic investigation along with the structural, compositional, and morphological analysis supported the outstanding visible light-induced catalytic behavior of phyto-synthesized nanomaterials. Moreover, the effects of visible light on degradation were confirmed by degrading MO in dark conditions which demonstrated that degradation of MO by synthesized catalysts was greatly enhanced in the presence of solar radiation. The reasons for this enhancement of photodegradation were increased oxygen valances of mixed metal oxides, carbon of the phyto-stabling agents, and n-p-type semiconducting materials. These factors tailored the electronic structures of the synthesized materials to enhance their catalytic activity for azo dyes degradation. Finally, the excellent reusability till four cycles of experiments revealed the huge potential of MoO_3:PdO and MoO_3:NiO as photocatalysts for industrial scale.

ACKNOWLEDGEMENTS

The authors acknowledge the Higher Education Commission of Pakistan, and Department of Environmental Sciences, Fatima Jinnah Women University Rawalpindi Pakistan. Authors profoundly acknowledge The University of Manchester UK for the providence of technical facilities. Authors declare no conflict of interest.

References

1) Zhong, W.; Jiang, T.; Dang, Y.; He, J.; Chen, S.-Y. Y.; Kuo, C.-H. H.; Kriz, D.; Meng, Y.; Meguerdichian, A. G.; Suib, S. L. Mechanism studies on methyl orange dye degradation by perovskite-type LaNiO3-δ under dark ambient conditions. *Applied Catalysis A: General* **2018**, *549*, 302–309.
2) Liú, D.; Wang, G.; Liǔ, D.; Lin, J.; He, Y.; Li, X.; Li, Z. Photocatalysis using zero-valent nano-copper for degrading methyl orange under visible light irradiation. *Optical Materials* **2016**, *53*, 155–159.
3) Suryavanshi, R. D.; Mohite, S. V.; Bagade, A. A.; Shaikh, S. K.; Thorat, J. B.; Rajpure, K. Y. Nanocrystalline immobilised ZnO photocatalyst for degradation of benzoic acid and methyl blue dye. *Materials Research Bulletin* **2018**, *101*, 324–333.
4) Zaman, M. B.; Poolla, R. Morphological tuning of hydrothermally derived visible light active Cu2SnS3 nanostructures and their applications in photocatalytic degradation of reactive industrial dyes. *Optical Materials* **2020**, *104*, 109853–109853.
5) Stubbs, N.; Bridgewater, M.; Stubbs, M.; Kabir, A.; Crescimanno, M.; Kuzyk, M. G.; Dawson, N. J. Polylactic acid promotes healing of photodegraded disperse orange 11 molecules. *Optical Materials* **2018**, *76*, 11–15.
6) He, K.; Chen, G.; Zeng, G.; Chen, A.; Huang, Z.; Shi, J.; Huang, T.; Peng, M.; Hu, L. . Three-dimensional graphene supported catalysts for organic dyes degradation. *Applied Catalysis B: Environmental* **2018**, *228*, 19–28.
7) Weeramonkhonlert, V.; Srikhaow, A.; Smith, S. M. Formation of copper hydroxy double salts derived from metal oxides and their catalytic activity in degradation of methyl orange. *Ceramics International* **2019**, *45* (1), 993–1000.
8) Araya, T.; Chen, C.-C. C.; Jia, M.-K. K.; Johnson, D.; Li, R.; Huang, Y.-P. P. Selective degradation of organic dyes by a resin modified Fe-based metal-organic framework under visible light irradiation. *Optical Materials* **2017**, *64*, 512–523.
9) Liang, H.; Tai, X.; Du, Z.; Yin, Y. Enhanced photocatalytic activity of ZnO sensitized by carbon quantum dots and application in phenol wastewater. *Optical Materials* **2020**, *100*, 109674–109674.
10) Mohammed, S. A.; Amouri, L. A.; Yousif, E. A.; Ali, A. A.; Mabood, F.; Abbas, H. F.; Alyaqoobi, S. Synthesis of NiO:V2O5 nanocomposite and its photocatalytic efficiency for methyl orange degradation. *Heliyon* **2018**, *4* (3), e00581–e00581.
11) Nasirian, M.; Mehrvar, M. Photocatalytic degradation of aqueous Methyl Orange using nitrogen-doped TiO 2 photocatalyst prepared by novel method of ultraviolet-assisted thermal synthesis. *Journal of Environmental Sciences* **2018**, *66*, 81–93.
12) Rani, M.; Shanker, U. Sun-light driven rapid photocatalytic degradation of methylene blue by poly(methyl methacrylate)/metal oxide nanocomposites. *Colloids and Surfaces A: Physicochemical and Engineering Aspects* **2018**, *559*, 136–147.
13) Hussain, M. K.; Khalid, N. R. Surfactant-assisted synthesis of MoO3 nanorods and its application in photocatalytic degradation of different dyes in aqueous environment. *Journal of Molecular Liquids* **2022**, *346*, 117871–117871.
14) Al-Alotaibi, A. L.; Altamimi, N.; Howsawi, E.; Elsayed, K. A.; Massoudi, I.; Ramadan, A. E. Synthesis and Characterization of MoO3 for Photocatalytic Applications. *Journal of Inorganic and Organometallic Polymers and Materials* **2021**, *31* (5), 2017–2029.
15) Zhang, Y.; Ping, X.; Hao, L.; He, Y.; Guo, Y.; Zhao, Q.; Zheng, Z.; Lu, Y. . Facile preparation of anodized MoO3−x films and their boosted photocatalytic activity. *Journal of Environmental Chemical Engineering* **2021**, *9* (4), 105565–105565.
16) Kamalam, M. B. R.; Inbanathan, S. S. R.; Sethuraman, K. Enhanced photo catalytic activity of graphene oxide /MoO3 nanocomposites in the degradation of Victoria Blue Dye under visible light irradiation. *Applied Surface Science* **2018**, *449*, 685–696.
17) Huang, Y.; Xing, W.; Zhou, L.; Tian, B.; Zhang, J.; Zhou, Y. Molybdenum oxide nanorods decorated with molybdenum phosphide quantum dots for efficient photocatalytic degradation of rhodamine B and norfloxacin. *Research on Chemical Intermediates* **2022**, *48* (7), 2887–2901.
18) Taymaz, B. H.; Eskizeybek, V.; Kamış, H. A novel polyaniline/NiO nanocomposite as a UV and visible-light photocatalyst for complete degradation of the model dyes and the real textile wastewater. *Environmental Science and Pollution Research* **2021**, *28* (6), 6700–6718.
19) Veziroglu, S.; Hwang, J.; Drewes, J.; Barg, I.; Shondo, J.; Strunskus, T.; Polonskyi, O.; Faupel, F.; Aktas, O. C. PdO nanoparticles decorated TiO2 film with enhanced photocatalytic and self-cleaning properties. *Materials Today Chemistry* **2020**, *16*, 100251–100251.
20) Zhou, W.; Guan, Y.; Wang, D.; Zhang, X.; Liu, D.; Jiang, H.; Wang, J.; Liu, X.; Liu, H.; Chen, S. . PdO/TiO2 and Pd/TiO2 Heterostructured Nanobelts with Enhanced Photocatalytic Activity. *Chemistry - An Asian Journal* **2014**, *9* (6), 1648–1654.
21) Kumar, H. N.; Mohana, N. C.; Nuthan, B. R.; Ramesha, K. P.; Rakshith, D.; Geetha, N.; Satish, S. Phyto-mediated synthesis of zinc oxide nanoparticles using aqueous plant extract of Ocimum americanum and evalu-

ation of its bioactivity. *SN Applied Sciences* **2019**, *1* (6), 651–651.
22) Zikalala, N.; Matshetshe, K.; Parani, S.; Oluwafemi, O. S.; Singh, J.; Dutta, T.; Kim, K. H.; Rawat, M.; Samddar, P.; Kumar, P. 'Green'synthesis of metals and their oxide nanoparticles: applications for environmental remediation. *Nano-Structures & Nano-Objects* **2018**, *16* (1), 84–84.
23) Banerjee, S.; Benjwal,; Singh, A.; Singh, N. B.; Afzal, S.; Singh, T.; Hussain, I. Zinc oxide nanoparticles: a review of their biological synthesis, antimicrobial activity, uptake, translocation and biotransformation in plants. *Journal of materials science* **2018**, *53* (1), 185–201.
24) Shaheen, I.; Ahmad, K. S. Green synthesis of doped Co3O4 nanocatalysts using organic template for fast azo dye degradation from aqueous environment. *Journal of Chemical Technology & Biotechnology* **2020**, *95* (11), 2898–2910.
25) Shaheen, I.; Ahmad, K. S.; Zequine, C.; Gupta, R. K.; Thomas, A.; Malik, M. A. Organic template-assisted green synthesis of CoMoO4 nanomaterials for the investigation of energy storage properties. *RSC Advances* **2020**, *10* (14), 8115–8129.
26) Zahra, T.; Ahmad, K. S.; Thomas, A. G.; Zequine, C.; Malik, M. A.; Gupta, R. K. Organic template-based ZnO embedded Mn3O4 nanoparticles: synthesis and evaluation of their electrochemical properties towards clean energy generation. *RSC Advances* **2020**, *10* (17), 9854–9867.
27) Krishna, A. G.; Ravikumar, R. V. S. S. N.; Kumar, T. V.; Ephraim, S. D.; Ranjith, B.; Pranoy, M.; Dola, S. Investigation and Comparison of Optical and Raman Bands of Mechanically Synthesised MoO3 Nano Powders. *Materials Today: Proceedings* **2016**, *3* (1), 54–63.
28) Joya, M. R.; Alfonso, J. E.; Moreno, L. C. Photoluminescence and Raman Studies of MoO3 Doped with Erbium and Neodymium. *Current Science* **2019**, *116* (10), 1690–1690.
29) Liu, H.; Cai, Y.; Han, M.; Guo, S.; Lin, M.; Zhao, M.; Zhang, Y.; Chi, D. . Aqueous and mechanical exfoliation, unique properties, and theoretical understanding of MoO3 nanosheets made from free-standing α-MoO3 crystals: Raman mode softening and absorption edge blue shift. *Nano Research* **2018**, *11* (3), 1193–1203.
30) Zhong, W.; Jiang, T.; Dang, Y.; He, J.; Chen, S.-Y. Y.; Kuo, C.-H. H.; Kriz, D.; Meng, Y.; Meguerdichian, A. G.; Suib, S. L. Mechanism studies on methyl orange dye degradation by perovskite-type LaNiO3-δ under dark ambient conditions. *Applied Catalysis A: General* **2018**, *549*, 302–309.
31) Ta, Q. T. H.; Cho, E.; Sreedhar, A.; Noh, J.-S. S. Mixed-dimensional, three-level hierarchical nanostructures of silver and zinc oxide for fast photocatalytic degradation of multiple dyes. *Journal of Catalysis* **2019**, *371*, 1–9.
32) Stengl, V.; Bakardjieva, S. Molybdenum-doped anatase and its extraordinary photocatalytic activity in the degradation of orange II in the UV and vis regions. *The Journal of Physical Chemistry C* **2010**, *114* (45), 19308–19317.
33) Chen, Y.; Lu, C.; Xu, L.; Ma, Y.; Hou, W.; Zhu, J.-J. J. Single-crystalline orthorhombic molybdenum oxide nanobelts: synthesis and photocatalytic properties. *CrystEngComm* **2010**, *12* (11), 3740–3740.
34) Munawar, K.; Mansoor, M. A.; Basirun, W. J.; Misran, M.; Huang, N. M.; Mazhar, M. Single step fabrication of CuO–MnO2–TiO2 composite thin films with improved photoelectrochemical response. *RSC Advances* **2017**, *7* (26), 15885–15893.
35) Reddy, K. R.; Gomes, V. G.; Hassan, M. Carbon functionalized TiO2 nanofibers for high efficiency photocatalysis. *Materials Research Express* **2014**, *1* (1), 015012–015012.
36) Li, W.; Zhao, S.; Qi, B.; Du, Y.; Wang, X.; Huo, M. Fast catalytic degradation of organic dye with air and MoO3:Ce nanofibers under room condition. *Applied Catalysis B: Environmental* **2009**, *92* (3-4), 333–340.
37) Srikhaow, A.; Smith, S. M. Preparation of Cu2(OH)3NO3/ZnO, a novel catalyst for methyl orange oxidation under ambient conditions. *Applied Catalysis B: Environmental* **2013**, *130-131*, 84–92.
38) Ren, H.; Gu, C.; Joo, S. W.; Zhao, J.; Sun, Y.; Huang, J. Effective hydrogen gas sensor based on NiO@rGO nanocomposite. *Sensors and Actuators B: Chemical* **2018**, *266*, 506–513.
39) Korifi, R.; Dréau, Y. L.; Molinet, J.; Artaud, J.; Dupuy, N. Composition and authentication of virgin olive oil from French PDO regions by chemometric treatment of Raman spectra. *Journal of Raman Spectroscopy* **2011**, *42* (7), 1540–1547.